Targeting Breast Tumors with pH (Low) Insertion Peptides

Ramona-Cosmina Adochite,[†] Anna Moshnikova,[†] Sean D. Carlin,[‡] Renato A. Guerrieri,[†] Oleg A. Andreev,[†] Jason S. Lewis,[‡,§] and Yana K. Reshetnyak*[,†]

[†]Physics Department, University of Rhode Island, 2 Lippitt Road, Kingston, Rhode Island 02881, United States

[‡]Department of Radiology and [§]Program in Molecular Pharmacology and Chemistry, Memorial Sloan-Kettering Cancer Center, 1275 York Avenue, New York, New York 10065, United States

S *Supporting Information*

ABSTRACT: Extracellular acidity is associated with tumor progression. Elevated glycolysis and acidosis promote the appearance of aggressive malignant cells with enhanced multidrug resistance. Thus, targeting of tumor acidity can open new avenues in diagnosis and treatment of aggressive tumors and targeting metastatic cancers cells within a tumor. pH (low) insertion peptides (pHLIPs) belong to the class of pH-sensitive agents capable of delivering imaging and/or therapeutic agents to cancer cells within tumors. Here, we investigated targeting of highly metastatic 4T1 mammary tumors and spontaneous breast tumors

Targeting of breast tumors in FVB/N-Tg (MMTV-PyMT)634Mul transgenic mice by pHLIP
Staining of non-malignant stromal tissues, shown by arrows, was minimal

H&E Histology | Hoechst Blood flow | Alexa546-pHLIP Var3-pHLIP | LDHA lactate dehydrogenase A | Pimonidazole hypoxia

in FVB/N-Tg (MMTV-PyMT)634Mul transgenic mice with three fluorescently labeled pHLIP variants including well-characterized WT-pHLIP and, recently introduced, Var3- and Var7-pHLIPs. The Var3- and Var7-pHLIPs constructs have faster blood clearance than the parent WT-pHLIP. All pHLIPs demonstrated excellent targeting of the above breast tumor models with tumor accumulation increasing over 4 h postinjection. Staining of nonmalignant stromal tissues in transgenic mice was minimal. The pHLIPs distribution in tumors showed colocalization with 2-deoxyglucose and the hypoxia marker, Pimonidazole. The highest degree of colocalization of fluorescent pHLIPs was shown to be with lactate dehydrogenase A, which is related to lactate production and acidification of tumors. In sum, the pHLIP-based targeting of breast cancer presents an opportunity to monitor metabolic changes, and to selectively deliver imaging and therapeutic agents to tumors.

KEYWORDS: *imaging, tumor acidity, glucose, lactate dehydrogenase, fluorescence, transgenic mice model*
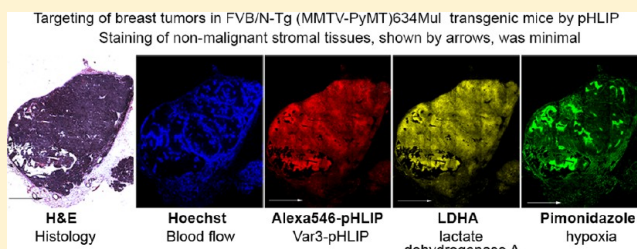
■ INTRODUCTION

For a wide variety of cancers, extracellular pH is significantly more acidic than in normal tissues. An acidic pH shift within solid tumors can regulate multiple biological processes such as proliferation, angiogenesis, immunosuppression, invasion, and chemoresistance.[1−6] Being a unique property of the majority of tumors, acidity may be heterogeneous within a single tumor.[7,8] This heterogeneity does not correlate spatially with tumor oxygenation; both well and poorly oxygenated parts of tumors can be acidic. Exposure of cancer cells to low pH has previously been shown to promote selection of stable, more invasive phenotypes.[6,9,10] Therefore, targeting tumor acidity might represent a novel approach for the prediction of tumor aggressiveness and delivery of therapeutic agents to tumor cells with the greatest metastatic potential.

Several pH-sensitive imaging and drug delivery systems have been introduced in which the release of the diagnostic or therapeutic agent is specifically triggered by the acidic tumor microenvironment.[11−15] Among these systems are peptides of the pHLIP (pH low insertion peptide) family, which represent a unique class of water-soluble membrane polypeptides capable of undergoing pH-dependent membrane-associated folding.[16,17] Transition of pHLIPs from the membrane-surface state at neutral pH to the membrane-inserted state at low pH is highly cooperative due to the accompanied coil−helix transformation within a lipid bilayer.[18−20] This pH-dependent insertion has been used for the targeting of imaging agents to acidic tumors, as well as translocation of polar cargo molecules across the phospholipid bilayer of the membrane of cancer cells; the well-characterized WT-pHLIP was employed for translocation of toxins and peptide nucleic acids into the cytoplasm of cancer cells, and for delivery of various imaging agents and targeting of both liposomes and gold nanoparticles to tumors and other acidic diseased tissue.[21−28] Biophysical investigations allowed us to broaden the chemical space of pHLIP peptides and establish rational design principles to define second generation constructs with the aim of clinical application. We introduced a family of novel pHLIP variants and demonstrated that tumor targeting, blood clearance, and biodistribution of these peptides can be modulated by tuning their sequence and, as a result, their physical and chemical properties and their interactions with the cell membrane.[18] The focus of our current research is a comparative study of the wild type (WT)-, Var3- and Var7-pHLIPs targeting of breast tumors.
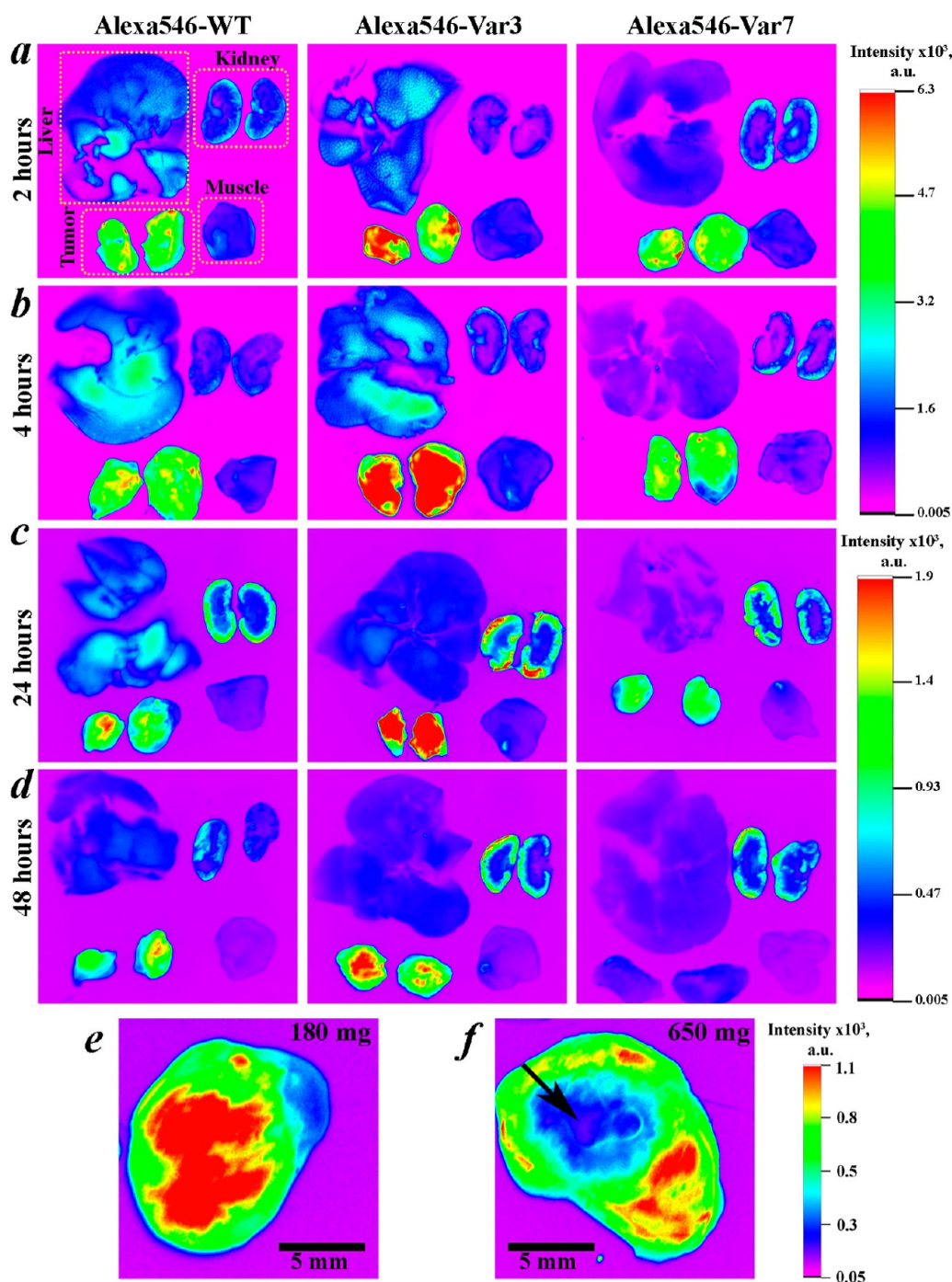
Figure 1. Distribution of pHLIPs in small 4T1 mammary tumors, muscle, kidney, and liver. Fluorescent images of organs obtained at 2 h (*a*), 4 h (*b*), 24 h (*c*), and 48 h (*d*) after intravenous administration of WT, Var3, and Var7 peptides conjugated with Alexa546 are shown. Distribution of pHLIPs is different in small (*e*) and big (*f*) 4T1 mammary tumors (tumor mass is indicated in upper right corner). The necrotic region of the big 4T1 mammary tumor is indicated by an arrow.

The data presented here provides important information about the pHLIPs distribution in tumors and colocalization with 2-deoxyglucose (2DG), lactate dehydrogenase A (an enzyme involved in lactate production), and the hypoxia marker, Pimonidazole.

■ MATERIALS AND METHODS

Synthesis and Labeling of Peptides. The pHLIP variants were prepared by solid-phase peptide synthesis using Fmoc (9-fluorenylmethyloxycarbonyl) chemistry and purified by

reverse phase chromatography by Dr. James I. Elliott at the W. M. Keck Foundation Biotechnology Resources Laboratory at Yale University (New Haven, CT). The pHLIP variants studied were as follows:

WT: ACEQNPIYWARYADWLFTTPLLLLLDLA-LLVDADEGT
Var3: ACDDQNPWRAYLDLLFPTDTLLLDLLW
Var7: ACEEQNPWARYLEWLFPTETLLLEL

The pHLIP variants were conjugated at the N-terminus with Alexa488-, Alexa546-, and Alexa647-maleimide (Life Technologies)

Table 1. Summary of the Experiments and Use of Fluorescent Constructs

study	use of fluorescent constructs
targeting of 4T1 mammary tumors, biodistribution, and histological analysis	Alexa546-WT, Alexa546-Var3, Alexa546-Var7
comparative study of distribution of three different pHLIPs in 4T1 mammary tumors (simultaneous administration of all fluorescent pHLIPs)	Alexa647-WT, Alexa546-Var3, Alexa448-Var7
targeting of transgenic breast tumors and histological analysis	IR680-WT, IR680-Var3, IR680-Var7, IR800-2DG

and IR680-maleimide (LiCor Biosciences) in DMF (dimethylformamide) at a ratio of 1:1 and incubated at room temperature for about 8 h and then at 4 °C until the conjugation was completed. The reaction progress was monitored by reverse phase (Zorbax SB-C18 columns, 9.4 × 250 mm 5 μm, Agilent Technology) high-performance liquid chromatography (HPLC) using gradients of 10−65% acetonitrile and water containing 0.05% of trifluoroacetic acid for Var3 and Var7 constructs and 10−75% acetonitrile and water containing 0.05% of trifluoroacetic acid for WT constructs. The products were lyophilized and characterized by SELDI-TOF mass spectrometry.

The concentrations of the constructs were determined by their absorbance using the following molar extinction coefficients: $\varepsilon_{495} = 71,000$ M^{-1}·cm^{-1} (for Alexa488-pHLIPs), $\varepsilon_{556} = 104,000$ M^{-1}·cm^{-1} (for Alexa546-pHLIPs), $\varepsilon_{650} = 239,000$ M^{-1}·cm^{-1} (for Alexa647-pHLIPs), and $\varepsilon_{672} = 165,000$ M^{-1}·cm^{-1} (for IR680-pHLIPs).

Cell Line. The 4T1 mouse mammary tumor cell line was obtained from the American Type Culture Collection and cultured in RPMI medium supplemented with 10% fetal bovine serum and 10 μg/mL of ciprofloxacin in a humidified atmosphere of 5% CO_2 and 95% air at 37 °C.

Tumor Mouse Models. All animal studies were conducted according to the animal protocol AN04-12-011 approved by the Institutional Animal Care and Use Committee at the University of Rhode Island, in compliance with the principles and procedures outlined by NIH for the Care and Use of Animals. 4T1 mammary tumors were established by subcutaneous injection of 4T1 cells (8 × 10^5 cells/0.1 mL/flank) in the right flank of adult female BALB/c mice (about 19−22 g weight) obtained from Harlan Laboratories. FVB/N-Tg(MMTV-PyVT)634Mul/J transgenic female mice (Jackson Laboratories) developed palpable mammary tumors at 12−15 weeks of age. Noncarrier FVB/NJ female mice (Jackson Laboratories), which did not develop mammary tumors, were used as a control mice.

Fluorescence Whole-Body and Organ Imaging. When tumors were palpable in the MMTV-Py MT mice, single tail vein injections of a cocktail of 1 nmol (100 μL of 10 μM) of IR680-labeled pHLIPs (WT, Var3, and Var7) and 10 nmol (100 μL of 100 μM) of IR800-labeled 2DG in PBS per mouse were performed. Control mice (noncarrier FVB/NJ) received the same dose of fluorescent pHLIPs (WT, Var3, and Var7) and 2DG. In xenografted BALB/c mice, tumors were used when they reached approximately 6 mm in diameter. Single tail vein injections of 5 nmol (100 μL of 50 μM) of Alexa488-, Alexa546-, and Alexa647-labeled pHLIPs in PBS (one pHLIP at the time or a cocktail of differently labeled pHLIPs) were performed. Pimonidazole, a marker of hypoxia (1.5 mg), and Hoechst 33342, a blood perfusion marker[29−32] (1 mg), were administered 1 h and 1.5 min before animal euthanization, respectively. Whole-body imaging followed by euthanization and necropsy was performed at 24 h postinjection. The whole-body imaging of transgenic mice was performed, while the animals were under ketamine/xylazine anesthesia and the skin was removed from the breast area. Animals were euthanized at 2, 4, 24, and 48 h postinjections followed by necropsy. Tumors and major organs of transgenic and BALB/c mice were imaged immediately after collection. The excised tumors were embedded in Tissue-Tek optimal cutting
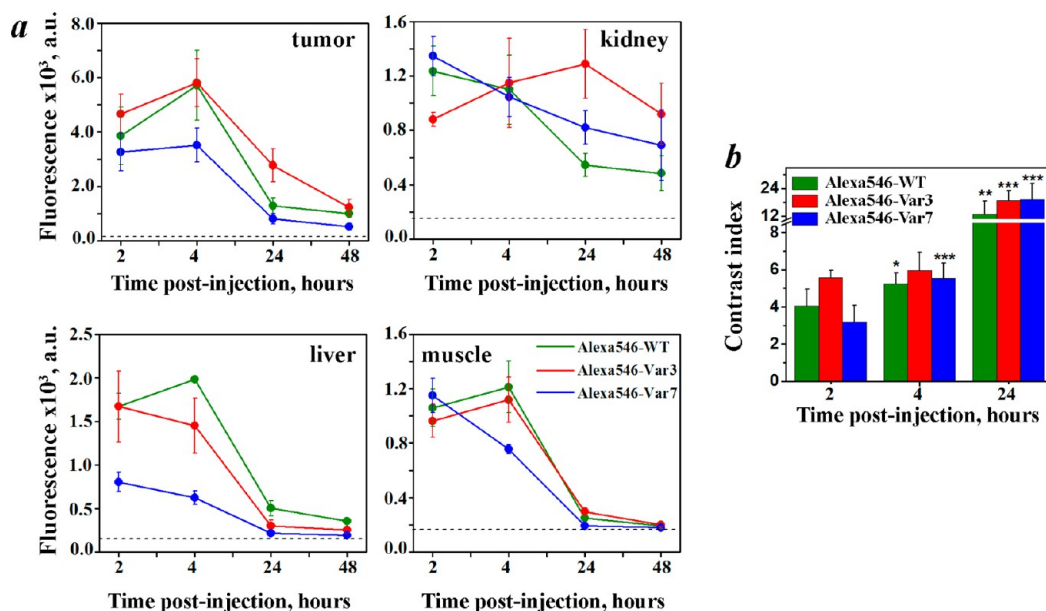

Figure 2. Time-dependent biodistribution of Alexa546-pHLIPs quantified by *ex vivo* mean fluorescence in 4T1 mammary tumors, muscle, kidney, and liver (*a*). The dashed lines indicate the level of autofluorescence signal. Contrast index was calculated for the 4T1 mammary tumors (*b*). The values are given in SI Tables 1 and 2, Supporting Information. Six mice per each Alexa-pHLIP constructs were used. The *p*-level values were computed based on the two-tailed test between means of CI at 2 vs 4 h and 2 vs 24 h for each pHLIP.
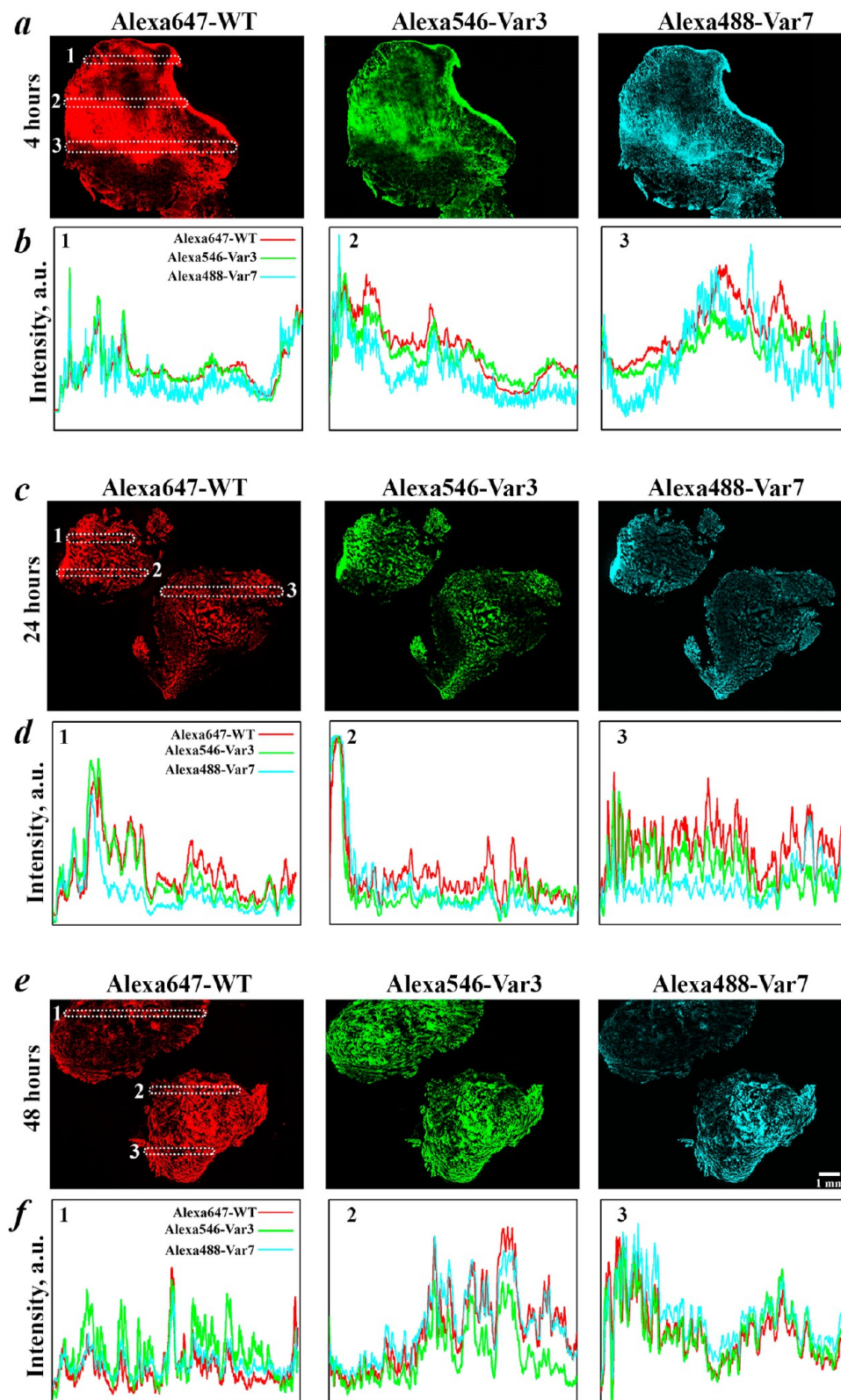
Figure 3. pHLIPs distribution in 4T1 mammary tumors. Fluorescence images of tumor sections for 4 h (*a*), 24 h (*c*), and 48 h (*e*) postinjections of cocktails of Alexa647-WT, Alexa546-Var3, and Alexa488-Var7 are shown. Intensity profiles of the fluorescent signal of various pHLIPs in the different lines are shown in panels *b*, *d*, and *f*.

temperature (OCT) compound and stored at −80 °C until used for immunohistochemical analysis.

Imaging of Alexa-pHLIPs and IR-pHLIPs/IR-2DG were carried out using a FX Kodak image station and an Odyssey IR scanner (Li-Cor Biosciences), respectively, using various magnifications and depth distances. Mean fluorescence intensity of tumor and organs was calculated using Kodak and ImageJ software. The contrast index (CI) was calculated according to the equation
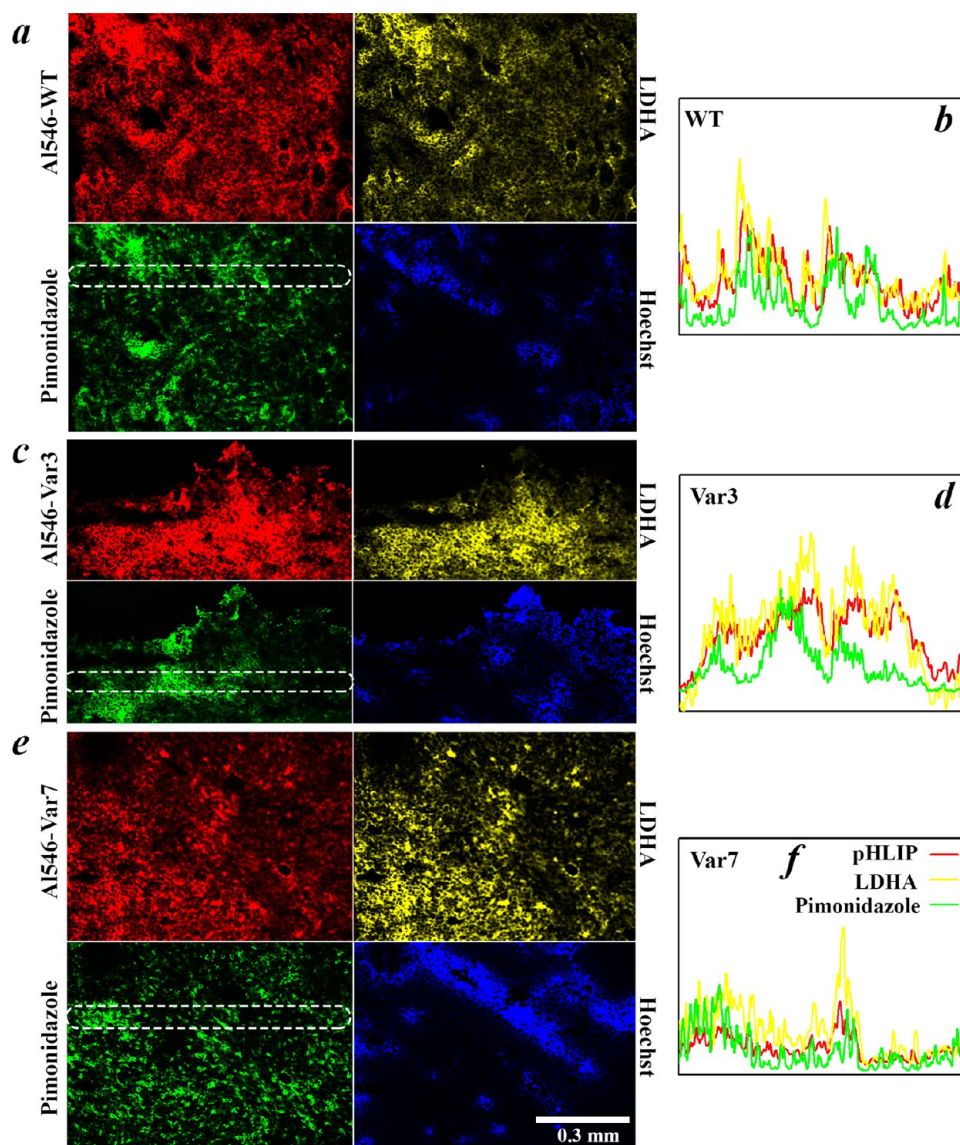
Figure 4. Immunohistochemical staining of 4T1 mammary tumors. pHLIPs distribution (Alexa546-pHLIPs, red), LDHA staining (yellow), hypoxia (Pimonidazole, green), and blood flow (Hoechst, blue) are compared on tumor sections (*a,c,e*). Intensity profiles of the fluorescent signals in the highlighted regions are shown in panels *b*, *d*, and *f*.

$$CI = \frac{F_{tumor} - F_{backg}}{F_{muscle} - F_{backg}}$$

where F_{tumor}, F_{muscle}, and F_{backg} are the mean fluorescence intensities of tumor, muscle, and background signals measured for control mice noninjected with fluorescent constructs.

Immunofluorescence Staining and Imaging of Tumor Sections. Frozen breast tumor tissues were sectioned at a thickness of 10 μm using a Vibratome UltraPro 5000 Cryostat. Sections were mounted on microscope slides, dried in air, and washed with deionized water. Tumor sections with the "pHLIPs-cocktail" were analyzed without further processing, while the remaining sections were fixed and stained. Slides were fixed in 4% paraformaldehyde (Sigma-Aldrich) for 12 min and washed with Dulbecco's Phosphate Buffered Saline (Life Technologies). The slides were dried in air and blocked using a mixture of 10% Goat serum (GeneTex), 1% bovine serum albumin (Life Technologies), and 0.3% Triton X-100 (Sigma-Aldrich) in phosphate buffered saline (Life Technologies) for 30 min. Then, immunofluorescence

staining for lactate dehydrogenase A (LDHA) and Pimonidazole was performed. For LDHA staining, rabbit polyclonal (NBP1-48336, Novus Biologicals) was used at 1:100 dilution, with goat antirabbit Alexa-568 (Life Technologies) at 1:100 for secondary detection. For Pimonidazole staining, FITC-conjugated mouse monoclonal anti-pimonidazole antibody (Natural Pharmacia International Inc.) was used at 1:20 dilution. Following fluorescence imaging, the same sections were then stained with hematoxylin and eosin (H&E).

Fluorescence and brightfield images were acquired at 4× magnification using an Olympus BX60 fluorescence microscope equipped with a motorized stage (Prior Scientific Instruments Ltd.) and coolsnap EZ CCD (Photometrics) and CC12 RGB camera (Olympus Scientific). Whole-tumor montage images were obtained by acquiring multiple fields, followed by alignment using MicroSuite Biologic Suite (version 2.7; Olympus).

■ **RESULTS**

In our study we used various tumor models and different fluorescent constructs. The summary is given in Table 1.
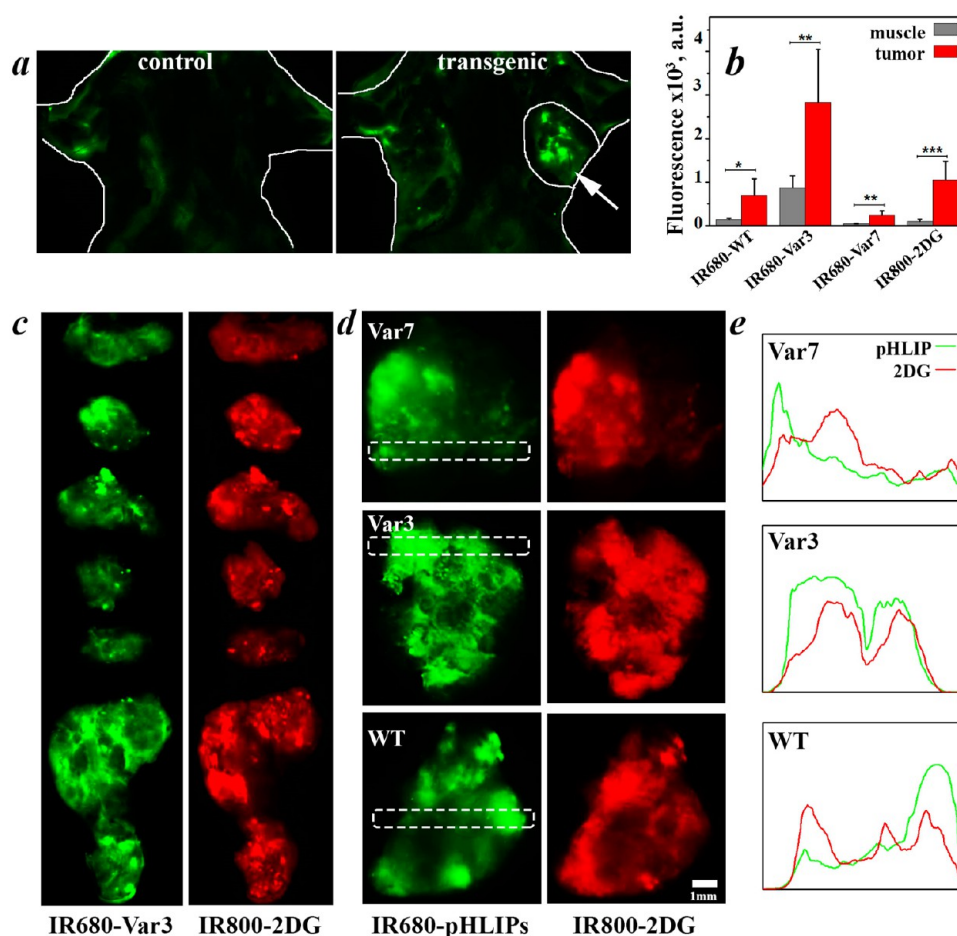
Figure 5. Tumor targeting by IR680-pHLIPs and IR800,2DG in transgenic mice. Whole-body NIR fluorescence images of control and transgenic mice were obtained at 24 h after intravenous administration of IR680-pHLIP, the contour of the mouse body is outlined, and the tumor is circled and indicated by arrow (*a*). Averaged mean fluorescence of IR680-pHLIPs and IR800-2DG in tumors, and muscle is calculated (*b*); the values are given in SI Table 3, Supporting Information. The *p*-level values were computed based on the two-tailed test. Distributions of IR680-pHLIPs (green) and IR800-2DG (red) in breast tumors are compared (*c,d*). Intensity profiles of the fluorescent pHLIPs and 2DG in the highlighted regions are shown in panel *e*.

Targeting 4T1 Mammary Tumors. The murine 4T1 xenograft model closely mimics stage IV of human breast cancer.[33−35] Small 4T1 mammary tumor (tumor volume < 150 mm^3) generates a significant level of lactate and serves as a good model of an aggressive, acidic tumor.[36] The pHLIP variants labeled with Alexa546 showed statistically significant targeting of tumors with minimal signal accumulation in liver, kidney, and muscle (Figures 1 and 2 and SI Table 1, Supporting Information). The signal in tumors continued to increase up to 4 h postinjection, and then declined within 48 h (Figure 2a and SI Table 1, Supporting Information). The highest uptake in tumor was observed for Var3; at 48 h postinjection the signal in tumor was still higher than the background fluorescence, while fluorescence in muscle and liver was at the level of autofluorescence. Var7 demonstrated fast clearance with steady decay of the fluorescent signal from 2 to 24 h in all organs except for the tumor, where the maximum signal was reached at 4 h postinjection. For Var3, the renal fluorescence signal was maximal at 24 h, indicating a slower clearance profile of this pHLIP variant. The optimal tumor targeting was achieved with Var3, which showed a statistically significant increase of a contrast index from 5 at 2−4 h to 19 at 24 h postinjection (Figure 2b). The statistically significant increase of contrast index for Var7 from 3 to 5 and up to 19 for 2, 4, and 24 h postinjection was observed, respectively. We did not

calculate the values of contrast index at 48 h since the signal in muscle were at background levels.

We compared the distribution of fluorescent-pHLIPs in both small (∼0.2 g) and necrotic large (∼0.5−0.6 g) 4T1 mammary tumors. The representative images of tumors (cut into halves) are shown in Figure 1e,f. In contrast to the smaller tumors, where the signal was homogeneously distributed within the entire tumor mass with maximal accumulation in the center of the tumor, the fluorescent signal in the necrotic core of the larger tumors was minimal.

Previously, we demonstrated the pH-dependent tumor targeting of WT-pHLIP.[27,28,37] Novel pHLIP variants also show pH-dependent tumor staining, but with different pharmacokinetics.[18] In this study, we compared the cellular localization and distribution of different pHLIPs in tumors. Frozen sections were prepared from tumors collected at 4, 24, and 48 h after administration of a cocktail of pHLIPs labeled with different fluorescent dyes: Alexa488-Var7, Alexa546-Var3, and Alexa647-WT given as a single tail vein injection (Figure 3). We selected later time points to minimize the concentration of the peptides in blood. The spatial distribution of all pHLIPs in tumors was identical. The intensity profiles for all pHLIPs obtained from the different areas of tumor sections were very similar, with minor differences in the background. Thus, despite
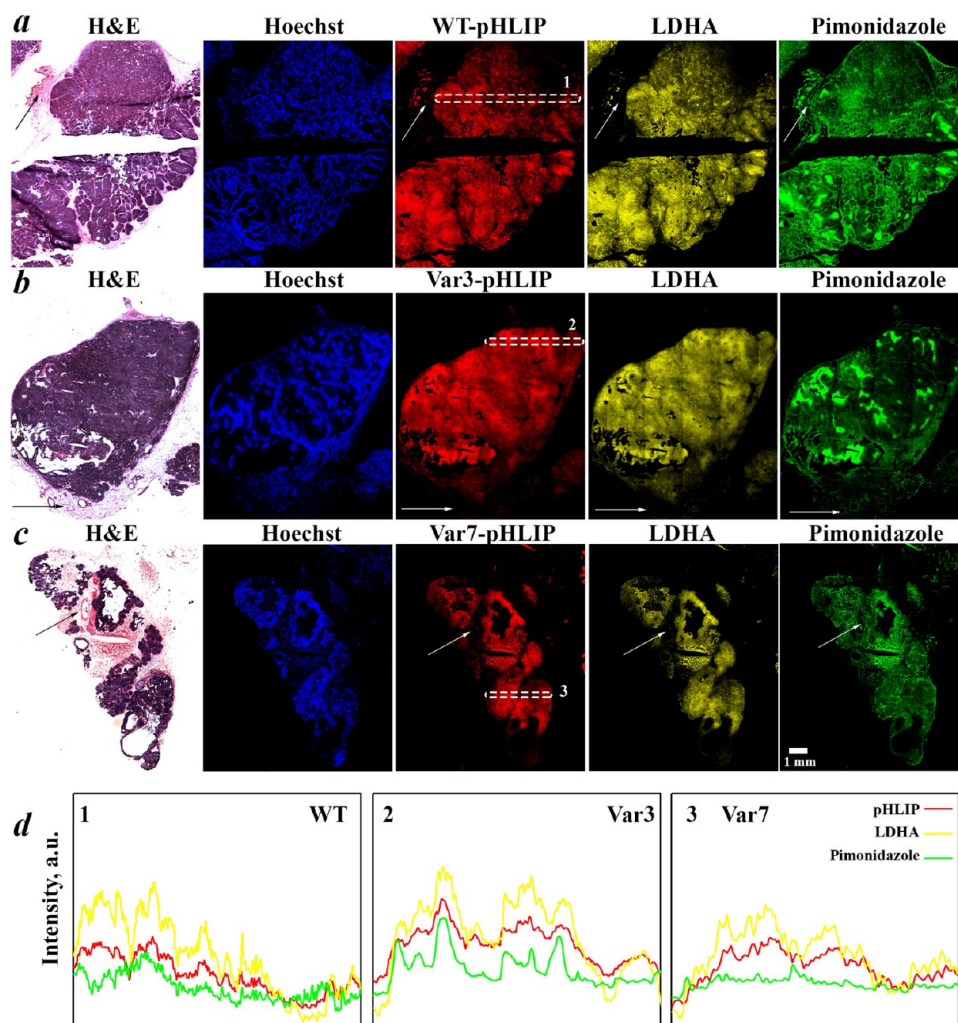
Figure 6. Immunohistochemical staining of tumors from transgenic mice. Histology (H&E), blood flow (Hoechst, blue), pHLIPs distribution (Alexa546-pHLIPs, red), LDHA staining (yellow), and hypoxia (Pimonidazole, green) are compared on tumor sections (*a−c*). The noncancerous regions are indicated by arrows. Intensity profiles of the fluorescent signals in the highlighted regions are shown in panel *d*.

the fact that pHLIP variants show different blood clearance profiles, the overall tumor spatial distributions were identical.

Immunohistochemical analysis of 4T1 mammary tumor sections revealed colocalization of fluorescent pHLIPs with hypoxia marker, Pimonidazole, and excellent colocalization with lactate dehydrogenase A (LDHA) (Figure 4).

Targeting Breast Tumors in Transgenic Mice. It has been established that breast tumor progression, from benign to metastatic disease, correlates with age in the FVB/N-Tg (MMTV-PyMT)634Mul transgenic mouse model,[38−40] with invasive tumors developing in mice of age 12 weeks and older. We used mice with an age range from 12 to 15 weeks to investigate distribution of pHLIPs in spontaneous invasive breast tumors. Tumor and organs were analyzed at 24 h after intravenous administration of Alexa546- or IR680-pHLIPs given as a single injection or in a mixture with the fluorescent nonmetabolizible 2DG. We observed pHLIP-targeting of breast tumors with a minimal level of fluorescence from control mice (noncarrier FVB/NJ female mice) or detectable signal in muscle at 24 h postinjection (Figure 5a,b). Higher tumor uptake of Var3 was observed, along with higher signal in muscle at 24 h compared to the other pHLIPs. The fluorescent signal for WT and Var7 was comparable to the signal from fluorescent 2DG, which was given at concentrations 10 times higher than for the

pHLIPs. Multiple tumors collected from the same mouse targeted by both IR680-Var3 and IR800-2DG are shown in Figure 5c; the heterogeneous distribution of IR800-2DG is apparent. Detailed analysis of the 2DG and pHLIPs distribution indicates that accumulation of 2DG correlates strongly with the accumulation of the pHLIPs (Figure 5d,e), but the pHLIPs also demonstrate targeting of additional regions.

Analysis of histological sections of breast tumors indicates that pHLIPs can clearly differentiate between regions of primarily tumor cells and nonmalignant stromal tissues (Figure 6a−c). Regions consisting mainly of tumor cells stained strongly with all pHLIP variants. Uptake of pHLIPs was observed in poorly perfused tumor regions (indicated by low Hoechst 33342 staining), which also accumulated the hypoxia marker Pimonidazole (Figures 6 and 7). However, we observed the highest degree of pHLIP colocalization with lactate dehydrogenase A (LDHA) enzyme, confirming that uptake of pHLIP is closely related to the production of acidic glucose metabolites in this model system.

■ DISCUSSION

Tumors of the same organ and cell type can have remarkably diverse appearances in different patients, which can restrict the use of targeting approaches based on overexpression of particular
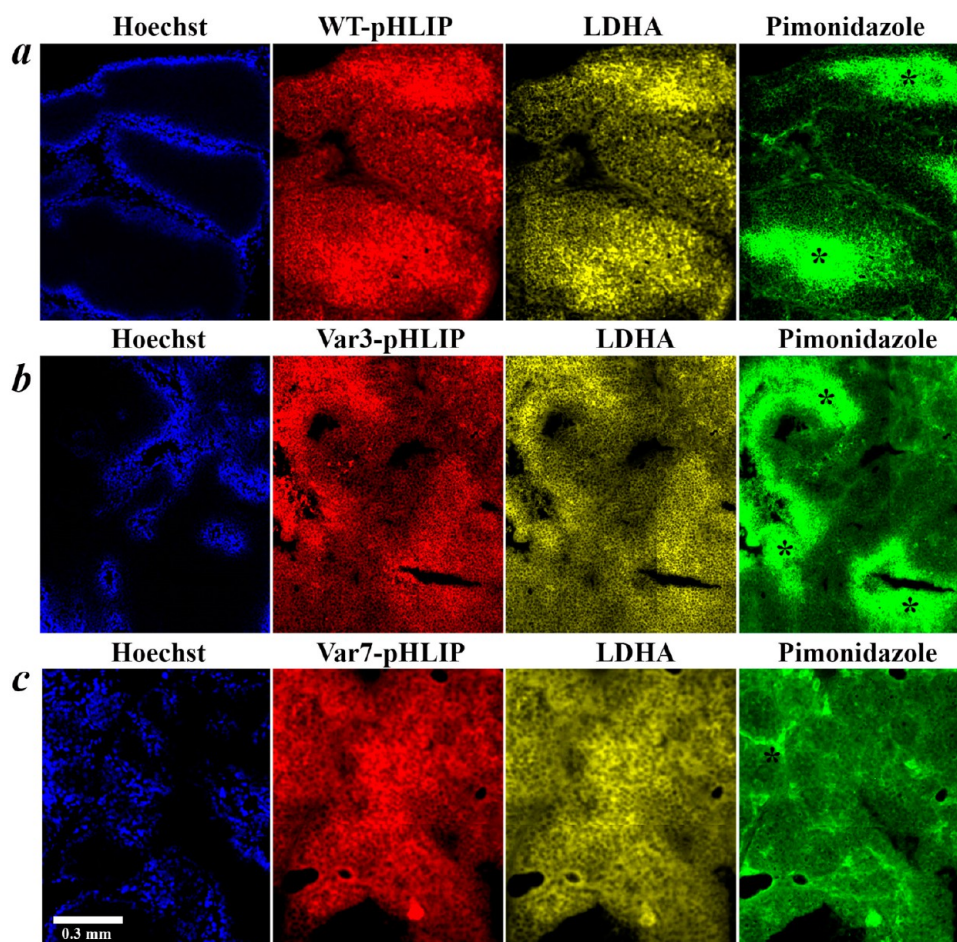
Figure 7. Magnified images of sections of breast tumors from transgenic mice. Blood flow (Hoechst, blue), pHLIPs distribution (Alexa546-pHLIPs, red), LDHA staining (yellow), and hypoxia (Pimonidazole, green) are compared on tumor sections (*a*−*c*). Hypoxic regions are indicated by stars.

protein biomarkers. Heterogeneity of the cancer cell population within a single tumor is assumed to lead to diminished treatment response. Cytotoxic therapies, while treating the majority of cancer cells, may spare multidrug resistant clones leading to tumor relapse and treatment failure.[41,42] Moreover, this transient depopulation of sensitive tumor cells by chemotherapeutic agents may provide a growth advantage to the surviving cells, leading to outgrowth of resistant clones.[42] It is therefore important to develop targeted imaging agents, which can reflect the underlying tumor microenvironment and allow for the targeted therapy of otherwise resistant cell clones. pH-responsive imaging and therapeutic probes could be particularly well-suited for this role as decreased extracellular pH is a general property of tumor microenvironments that is also reflective of tumor aggressiveness since most malignant cells within a tumor mass are glycolytic and acidic.

Previously we demonstrated that the water-soluble membrane peptide, WT-pHLIP, can deliver optical, PET, and SPECT imaging agents to the primary tumors and metastatic lesions in a pH-dependent manner and distinguish between aggressive and nonmetastatic tumors.[26−28,37] Here we show that both 4T1 mammary tumors and breast tumors in transgenic mice were targeted very well by all fluorescently labeled pHLIP variants, with minimal signal observed in other organs, stroma, or necrotic 4T1 mammary tumors, which have a lower level of lactate production.[36] Var3 and Var7 were recently introduced as novel pHLIP variants, which show higher tumor targeting and fast blood clearance, respectively,[18] and are able to target pancreatic

tumors in various mouse models.[43] Despite the difference in pharmacokinetics of pHLIP variants, Var3 and Var7 demonstrate distribution in tumors identical to the well-characterized WT-pHLIP.

Using IR800-2DG we observed that the spatial distribution of the glucose analogue in tumors is heterogeneous, and this correlated well with the pHLIPs distribution. Regions of elevated pHLIPs uptake correlated with the hypoxia marker Pimonidazole as well. At the same time, pHLIPs also target adjacent regions to the 2DG uptake and showed accumulation in nonhypoxic tumor regions. The highest colocalization of pHLIPs was seen with lactate dehydrogenase A in both transgenic and 4T1 small mammary tumors. LDHA expression is partially regulated by the hypoxia-inducible HIF1 transcription factor, as is the glucose transporter GLUT-1. Increased LDHA expression, with consequent increased lactate production and generation of hydrogen ions, would be expected to correlate most closely with pH-dependent uptake of pHLIP, as was observed in this study. Our observation of a positive correlation between pHLIP uptake and markers of glucose transport and metabolism strongly implies that pHLIP is specifically accumulated in tumor regions displaying typical characteristics of a stressed microenvironment, such as hypoxia, elevated glucose uptake, and glycolytic metabolism.

Despite an evident correlation between 2DG uptake, lactate production, and tumor acidification, it was shown that 2-deoxy-2-[^{18}F]fluoro-D-glucose positron emission tomography ([^{18}F]FDG-PET) imaging was significantly less sensitive to differences in the

metabolic phenotypes of tumors compared to the lactate-magnetic resonance spectroscopic imaging (MRSI).[36] Although MRSI can provide additional information about metabolic activities in tumors, it is not yet widely implemented in a clinical setting. The potential therefore exists for pHLIP to provide imaging data of a similar nature to lactate-MRSI, but with a clearer path to rapid clinical translation. Use of any of the three pHLIP variants labeled with PET or SPECT agents (e.g., ^{18}F, ^{64}Cu, and ^{99}Tc) could allow monitoring of metabolic changes in human tumors over time or in response to therapeutic intervention. In addition, pHLIP peptides could be used for delivery of therapeutic cargoes to tumors, which might target the most aggressive cancer cell clones.

■ ASSOCIATED CONTENT

Ⓢ Supporting Information

Mean fluorescence and contrast index. This material is available free of charge via the Internet at http://pubs.acs.org.

■ AUTHOR INFORMATION

Corresponding Author

*(Y.K.R.) E-mail: reshetnyak@mail.uri.edu.

Notes

The authors declare no competing financial interest.

■ ACKNOWLEDGMENTS

■ ABBREVIATIONS USED

2DG, 2-deoxyglucose; CCD, charge-couples device; CI, contrast index; FDG, 2-deoxy-2-fluoro-D-glucose; FITC, fluorescein isothiocyanate; HPLC, high pressure liquid chromatography; h, hours; IR, infrared; LHDA, lactate dehydrogenase A; MRSI, magnetic resonance spectroscopic imaging; NIH, National Institutes of Health; PBS, phosphate buffer saline; PET, positron emission tomography; pHLIP, pH low insertion peptide; RMPI, Roswell Park Memorial Institute medium; SELDI-TOF, surface enhanced laser desorption/ionization time-of-flight; SPECT, single photon emission computed tomography; Var, variant; WT, wild type

■ REFERENCES

(1) Kallinowski, F.; Vaupel, P. pH distributions in spontaneous and isotransplanted rat tumours. *Br. J. Cancer* **1988**, *58* (3), 314−21.

(2) Lessi, E.; Marino, M. L.; Lozupone, F.; Fais, S.; De Milito, A. Tumor acidity and malignancy: novel aspects in the design of anti-tumor therapy. *Cancer Ther.* **2008**, *6*, 55−66.

(3) Vaupel, P.; Kallinowski, F.; Okunieff, P. Blood flow, oxygen and nutrient supply, and metabolic microenvironment of human tumors: a review. *Cancer Res.* **1989**, *49* (23), 6449−65.

(4) Gerweck, L. E.; Seetharaman, K. Cellular pH gradient in tumor versus normal tissue: potential exploitation for the treatment of cancer. *Cancer Res.* **1996**, *56* (6), 1194−8.

(5) Bhujwalla, Z. M.; Artemov, D.; Ballesteros, P.; Cerdan, S.; Gillies, R. J.; Solaiyappan, M. Combined vascular and extracellular pH imaging of solid tumors. *NMR Biomed.* **2002**, *15* (2), 114−9.

(6) Gatenby, R. A.; Gawlinski, E. T.; Gmitro, A. F.; Kaylor, B.; Gillies, R. J. Acid-mediated tumor invasion: a multidisciplinary study. *Cancer Res.* **2006**, *66* (10), 5216−23.

(7) Garcia-Martin, M. L.; Martinez, G. V.; Raghunand, N.; Sherry, A. D.; Zhang, S.; Gillies, R. J. High resolution pH(e) imaging of rat glioma using pH-dependent relaxivity. *Magn. Reson. Med.* **2006**, *55* (2), 309−15.

(8) Gillies, R. J.; Raghunand, N.; Garcia-Martin, M. L.; Gatenby, R. A. pH imaging. A review of pH measurement methods and applications in cancers. *IEEE Eng. Med. Biol. Mag.* **2004**, *23* (5), 57−64.

(9) Reichert, M.; Steinbach, J. P.; Supra, P.; Weller, M. Modulation of growth and radiochemosensitivity of human malignant glioma cells by acidosis. *Cancer* **2002**, *95* (5), 1113−9.

(10) Moellering, R. E.; Black, K. C.; Krishnamurty, C.; Baggett, B. K.; Stafford, P.; Rain, M.; Gatenby, R. A.; Gillies, R. J. Acid treatment of melanoma cells selects for invasive phenotypes. *Clin. Exp. Metastasis* **2008**, *25* (4), 411−25.

(11) He, X.; Li, J.; An, S.; Jiang, C. pH-sensitive drug-delivery systems for tumor targeting. *Ther. Delivery* **2013**, *4* (12), 1499−510.

(12) Budker, V.; Gurevich, V.; Hagstrom, J. E.; Bortzov, F.; Wolff, J. A. pH-sensitive, cationic liposomes: a new synthetic virus-like vector. *Nat. Biotechnol.* **1996**, *14* (6), 760−4.

(13) Chen, D.; Jiang, X.; Liu, J.; Jin, X.; Zhang, C.; Ping, Q. In vivo evaluation of novel pH-sensitive mPEG-Hz-Chol conjugate in liposomes: pharmacokinetics, tissue distribution, efficacy assessment. *Artif. Cells, Blood Substitutes, Immobilization Biotechnol.* **2010**, *38* (3), 136−42.

(14) Han, L.; Guo, Y.; Ma, H.; He, X.; Kuang, Y.; Zhang, N.; Lim, E.; Zhou, W.; Jiang, C. Acid active receptor-specific peptide ligand for in vivo tumor-targeted delivery. *Small* **2013**, *9*, 3647−58.

(15) Zhang, S.; Wu, K.; Sherry, A. D. A Novel pH-Sensitive MRI Contrast Agent. *Angew. Chem., Int. Ed.* **1999**, *38* (21), 3192−3194.

(16) Andreev, O. A.; Engelman, D. M.; Reshetnyak, Y. K. pH-sensitive membrane peptides (pHLIPs) as a novel class of delivery agents. *Mol. Membr. Biol.* **2010**, *27* (7), 341−52.

(17) Andreev, O. A.; Engelman, D. M.; Reshetnyak, Y. K. Targeting diseased tissues by pHLIP insertion at low cell surface pH. *Front. Physiol.* **2014**, *5*, 97.

(18) Weerakkody, D.; Moshnikova, A.; Thakur, M. S.; Moshnikova, V.; Daniels, J.; Engelman, D. M.; Andreev, O. A.; Reshetnyak, Y. K. Family of pH (low) insertion peptides for tumor targeting. *Proc. Natl. Acad. Sci. U.S.A.* **2013**, *110* (15), 5834−9.

(19) Karabadzhak, A. G.; Weerakkody, D.; Wijesinghe, D.; Thakur, M. S.; Engelman, D. M.; Andreev, O. A.; Markin, V. S.; Reshetnyak, Y. K. Modulation of the pHLIP transmembrane helix insertion pathway. *Biophys. J.* **2012**, *102* (8), 1846−55.

(20) Andreev, O. A.; Karabadzhak, A. G.; Weerakkody, D.; Andreev, G. O.; Engelman, D. M.; Reshetnyak, Y. K. pH (low) insertion peptide (pHLIP) inserts across a lipid bilayer as a helix and exits by a different path. *Proc. Natl. Acad. Sci. U.S.A.* **2010**, *107* (9), 4081−6.

(21) Yao, L.; Daniels, J.; Wijesinghe, D.; Andreev, O. A.; Reshetnyak, Y. K. pHLIP(R)-mediated delivery of PEGylated liposomes to cancer cells. *J. Controlled Release* **2013**, *167* (3), 228−237.

(22) Yao, L.; Daniels, J.; Moshnikova, A.; Kuznetsov, S.; Ahmed, A.; Engelman, D. M.; Reshetnyak, Y. K.; Andreev, O. A. pHLIP peptide targets nanogold particles to tumors. *Proc. Natl. Acad. Sci. U.S.A.* **2013**, *110* (2), 465−70.

(23) Wijesinghe, D.; Arachchige, M. C.; Lu, A.; Reshetnyak, Y. K.; Andreev, O. A. pH dependent transfer of nano-pores into membrane of cancer cells to induce apoptosis. *Sci. Rep.* **2013**, *3*, 3560.

(24) Moshnikova, A.; Moshnikova, V.; Andreev, O. A.; Reshetnyak, Y. K. Antiproliferative effect of pHLIP-amanitin. *Biochemistry* **2013**, *52* (7), 1171−8.

(25) Daumar, P.; Wanger-Baumann, C. A.; Pillarsetty, N.; Fabrizio, L.; Carlin, S. D.; Andreev, O. A.; Reshetnyak, Y. K.; Lewis, J. S. Efficient (18)F-labeling of large 37-amino-acid pHLIP peptide analogues and their biological evaluation. *Bioconjugate Chem.* **2012**, *23* (8), 1557−66.

(26) Reshetnyak, Y. K.; Yao, L.; Zheng, S.; Kuznetsov, S.; Engelman, D. M.; Andreev, O. A. Measuring tumor aggressiveness and targeting metastatic lesions with fluorescent pHLIP. *Mol. Imaging Biol.* **2011**, *13* (6), 1146−56.

(27) Vavere, A. L.; Biddlecombe, G. B.; Spees, W. M.; Garbow, J. R.; Wijesinghe, D.; Andreev, O. A.; Engelman, D. M.; Reshetnyak, Y. K.; Lewis, J. S. A novel technology for the imaging of acidic prostate tumors by positron emission tomography. *Cancer Res.* **2009**, *69* (10), 4510−6.

(28) Macholl, S.; Morrison, M. S.; Iveson, P.; Arbo, B. E.; Andreev, O. A.; Reshetnyak, Y. K.; Engelman, D. M.; Johannesen, E. In vivo pH imaging with (99m)Tc-pHLIP. *Mol. Imaging Biol.* **2012**, *14* (6), 725−34.

(29) Olive, P. L.; Chaplin, D. J.; Durand, R. E. Pharmacokinetics, binding and distribution of Hoechst 33342 in spheroids and murine tumours. *Br. J. Cancer* **1985**, *52* (5), 739−46.

(30) Oehler, C.; O'Donoghue, J. A.; Russell, J.; Zanzonico, P.; Lorenzen, S.; Ling, C. C.; Carlin, S. 18F-fluromisonidazole PET imaging as a biomarker for the response to 5,6-dimethylxanthenone-4-acetic acid in colorectal xenograft tumors. *J. Nucl. Med.* **2011**, *52* (3), 437−44.

(31) Carlin, S.; Khan, N.; Ku, T.; Longo, V. A.; Larson, S. M.; Smith-Jones, P. M. Molecular targeting of carbonic anhydrase IX in mice with hypoxic HT29 colorectal tumor xenografts. *PLoS One* **2010**, *5* (5), e10857.

(32) Li, X. F.; Carlin, S.; Urano, M.; Russell, J.; Ling, C. C.; O'Donoghue, J. A. Visualization of hypoxia in microscopic tumors by immunofluorescent microscopy. *Cancer Res.* **2007**, *67* (16), 7646−53.

(33) Tao, K.; Fang, M.; Alroy, J.; Sahagian, G. G. Imagable 4T1 model for the study of late stage breast cancer. *BMC Cancer* **2008**, *8*, 228.

(34) Yang, J.; Mani, S. A.; Donaher, J. L.; Ramaswamy, S.; Itzykson, R. A.; Come, C.; Savagner, P.; Gitelman, I.; Richardson, A.; Weinberg, R. A. Twist, a master regulator of morphogenesis, plays an essential role in tumor metastasis. *Cell* **2004**, *117* (7), 927−39.

(35) Eckhardt, B. L.; Parker, B. S.; van Laar, R. K.; Restall, C. M.; Natoli, A. L.; Tavaria, M. D.; Stanley, K. L.; Sloan, E. K.; Moseley, J. M.; Anderson, R. L. Genomic analysis of a spontaneous model of breast cancer metastasis to bone reveals a role for the extracellular matrix. *Mol. Cancer Res.* **2005**, *3* (1), 1−13.

(36) Serganova, I.; Rizwan, A.; Ni, X.; Thakur, S. B.; Vider, J.; Russell, J.; Blasberg, R.; Koutcher, J. A. Metabolic imaging: a link between lactate dehydrogenase A, lactate, and tumor phenotype. *Clin. Cancer Res.* **2011**, *17* (19), 6250−61.

(37) Andreev, O. A.; Dupuy, A. D.; Segala, M.; Sandugu, S.; Serra, D. A.; Chichester, C. O.; Engelman, D. M.; Reshetnyak, Y. K. Mechanism and uses of a membrane peptide that targets tumors and other acidic tissues in vivo. *Proc. Natl. Acad. Sci. U.S.A.* **2007**, *104* (19), 7893−8.

(38) Hutchinson, J. N.; Muller, W. J. Transgenic mouse models of human breast cancer. *Oncogene* **2000**, *19* (53), 6130−7.

(39) Guy, C. T.; Cardiff, R. D.; Muller, W. J. Induction of mammary tumors by expression of polyomavirus middle T oncogene: a transgenic mouse model for metastatic disease. *Mol. Cell. Biol.* **1992**, *12* (3), 954−61.

(40) Lin, E. Y.; Jones, J. G.; Li, P.; Zhu, L.; Whitney, K. D.; Muller, W. J.; Pollard, J. W. Progression to malignancy in the polyoma middle T oncoprotein mouse breast cancer model provides a reliable model for human diseases. *Am. J. Pathol.* **2003**, *163* (5), 2113−26.

(41) Cheng, G. M.; To, K. K. Adverse cell culture conditions mimicking the tumor microenvironment upregulate ABCG2 to mediate multidrug resistance and a more malignant phenotype. *ISRN Oncol.* **2012**, *2012*, 746025.

(42) Gatenby, R. A.; Silva, A. S.; Gillies, R. J.; Frieden, B. R. Adaptive therapy. *Cancer Res.* **2009**, *69* (11), 4894−903.

(43) Cruz-Monserrate, Z.; Roland, C. L.; Deng, D.; Arumugam, T.; Moshnikova, A.; Andreev, O. A.; Reshetnyak, Y. K.; Logsdon, C. D. Targeting pancreatic ductal adenocarcinoma acidic microenvironment. *Sci. Rep.* **2014**, *4*, 4410.